PROCEEDINGS OF SCIENCE

Production of exclusive dijets in diffractive deep inelastic scattering at HERA

Leszek ADAMCZYK[*†] **on behalf of the ZEUS Collaboration**
AGH University of Science and Technology, Faculty of Physics and Applied Computer Science, Cracow, Poland
E-mail: leszek.adamczyk@agh.edu.pl

Production of exclusive dijets in diffractive deep inelastic $e^{\pm}p$ scattering has been measured with the ZEUS detector at HERA using an integrated luminosity of 372 pb^{-1}. The measurement was performed for γ^*–p centre-of-mass energies in the range $90 < W < 250$ GeV and for photon virtualities $Q^2 > 25$ GeV^2. Energy and transverse-energy flows around the jet axis are presented. The cross section is presented as a function of β and ϕ, where $\beta = x/x_{\mathbb{P}}$, x is the Bjorken variable and $x_{\mathbb{P}}$ is the proton fractional longitudinal momentum loss. The angle ϕ is defined by the γ^*–dijet plane and the γ^*–$e^{\pm}$ plane in the rest frame of the diffractive final state. The ϕ cross section is measured in bins of β. The results are compared to predictions from models based on different assumptions about the nature of the diffractive exchange.

XXIII International Workshop on Deep-Inelastic Scattering
27 April - May 1 2015
Dallas, Texas

[*]Speaker.
[†]This work was partly supported by the Polish NCN grant nr UMO-2012/06/M/ST2/00428

PoS(DIS2015)062

1. Introduction

The first evidence for exclusive dijet production at high-energy hadron colliders was provided by the CDF experiment at the Fermilab Tevatron $p\bar{p}$ collider [1] and had an important impact on theoretical calculations of exclusive Higgs boson production at the Large Hadron Collider. This paper describes the first measurement of exclusive dijet production in high energy electron[1]–proton scattering. A quantitative understanding of the production of exclusive dijets in lepton–hadron scattering can improve the understanding of more complicated processes like the exclusive production of dijets in hadron–hadron scattering [2] or in lepton–ion scattering at a future eRHIC accelerator [3].

A schematic view of the diffractive production of exclusive dijets, $e+p \to e+\text{jet1}+\text{jet2}+p$, is shown in Fig. 1. In this picture, electron–proton deep inelastic scattering (DIS) is described in terms of an interaction between the virtual photon, γ^*, and the proton, which is mediated by the exchange of a colourless object called the Pomeron ($\mathbb{P}$). This process in the γ^*–$\mathbb{P}$ centre-of-mass frame is presented in Fig. 2, where the lepton and jet planes are marked. The lepton plane is defined by the incoming and scattered electron momenta. The jet plane is defined by the jet momenta, which are always back-to-back, and the virtual photon momentum. The angle between these planes is labelled ϕ. The jet polar angle is defined with respect to the virtual photon momentum and called θ. Calculations of the single-differential cross section of dijet production as a function of ϕ in k_t-factorisation [4] and collinear factorisation [5] have shown that the cross section is proportional to $1+A(p_{T,\text{jet}})\cos 2\phi$, where $p_{T,\text{jet}}$ is the jet transverse momentum.

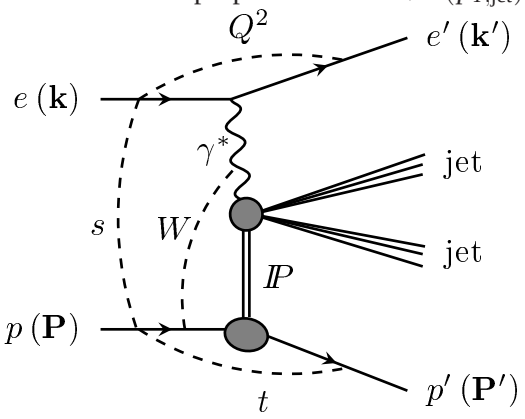

Figure 1: Schematic view of the diffractive production of exclusive dijets in electron–proton DIS.

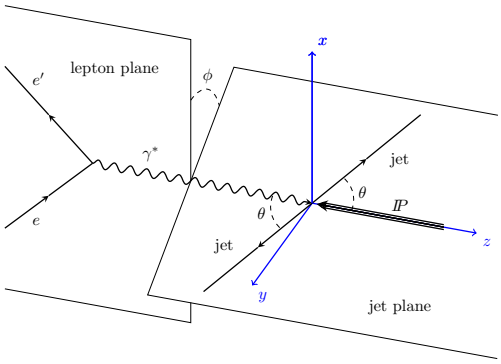

Figure 2: Definition of planes and angles in the γ^*-$\mathbb{P}$ centre-of-mass system.

This paper describes the measurement of differential cross sections as a function of β and in bins of β as a function of ϕ. The former quantity is defined as $\beta = x/x_{\mathbb{P}}$, where x is the Bjorken variable and $x_{\mathbb{P}}$ is the fractional loss of proton longitudinal momentum. The results of this analysis are compared to predictions from the Two-Gluon-Exchange model [6, 7] and the Resolved-Pomeron model of Ingelman and Schlein [8].

[1]Here and in the following the term "electron" denotes generically both the electron and the positron.

2. Event selection and reconstruction

This analysis is based on data collected with the ZEUS detector at the HERA collider during the 2003–2007 data-taking period, when electrons or positrons of 27.5 GeV were collided with protons of 920 GeV at a centre-of-mass energy of $\sqrt{s} = 318$ GeV. The data sample corresponds to an integrated luminosity of 372 pb^{-1}. Energy-flow objects (EFOs [9, 10]) were used to combine the information from the calorimiter (CAL) and the central tracking detector (CTD).

2.1 DIS selection

A clean sample of DIS events with a well-reconstructed electron was selected by the following criteria:

- the electron candidate was required to have an energy $E'_e > 10$ GeV and, if reconstructed in the CTD acceptance region, also an associated track;
- the reconstructed position of the electron candidate in the CAL was required to be outside the regions of CAL in which the scattered electron might have crossed a substantial amount of inactive material or regions with poor acceptance;
- the vertex position along the beam axis was required to be in the range $|Z_{\text{vtx}}| < 30$ cm;
- $E_{\text{had}}/E_{\text{tot}} > 0.06$, where E_{had} is the energy deposited in the hadronic part of the CAL and E_{tot} is the total energy in the CAL; this cut removes purely electromagnetic events;
- $45 < (E - P_Z) < 70$ GeV, where E is the total energy, $E = \sum_i E_i$, $P_Z = \sum_i p_{Z,i}$ and $p_{Z,i} = E_i \cos\theta_i$, where the sums run over all EFOs including the electron; this cut removes events with large initial-state radiation and further reduces the background from photoproduction.

Events were accepted if $Q^2 > 25$ GeV^2 and $90 < W < 250$ GeV.

2.2 Diffractive selection

Diffractive events are characterised by a small momentum exchange at the proton vertex and by the presence of a large rapidity gap (LRG) between the proton beam direction and the hadronic final state. Diffractive DIS events were selected by the following additional criteria:

- $x_{\mathbb{P}} < 0.01$, where $x_{\mathbb{P}}$ is the fraction of the proton momentum carried by the diffractive exchange, calculated according to the formula $x_{\mathbb{P}} = \left(Q^2 + M_X^2\right) / \left(Q^2 + W^2\right)$, in which M_X denotes the invariant mass of the hadronic state recoiling against the leading proton and was reconstructed from the EFOs excluding the scattered electron candidate; this cut reduces the non-diffractive background;
- $\eta_{\text{max}} < 2$, where η_{max} is defined as the pseudorapidity of the most forward EFO, with an energy greater than $E_{\text{EFO}} = 400$ MeV; this cut ensures the presence of a LRG in the event;
- $M_X > 5$ GeV; this cut removes events with resonant particle production and ensures that there is enough energy in the system to create two jets with high transverse momenta.

The data were analysed as a function of β, calculated according to $\beta = Q^2 / \left(Q^2 + M_X^2\right)$.

2.3 Jet selection

The k_T-cluster algorithm known as the Durham jet algorithm [11, 12], as implemented in the FastJet package [13], was used for jet reconstruction. It was run in exclusive mode i.e. each object had to be finally associated to a jet. The algorithm is defined in the following way: first all objects were boosted to the γ^*–$\mathbb{P}$ rest frame. Then, the relative distance of each pair of objects, $k^2_{T\,ij}$, was calculated as

$$k^2_{T\,ij} = 2\min(E_i^2, E_j^2)(1-\cos\theta_{ij}),$$

where θ_{ij} is the angle between objects i and j and E_i and E_j are the energies of the objects i and j. The minimum $k^2_{T\,ij}$ was found and if

$$y_{ij} = \frac{k^2_{T\,ij}}{M_X^2} < y_{\rm cut}$$

objects i and j were merged. The same jet-search procedure was applied to the final-state hadrons for simulated events.

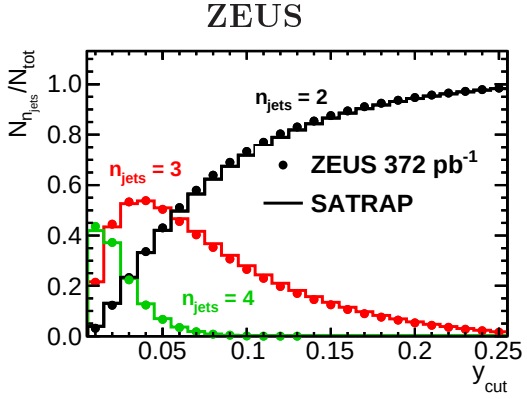

Figure 3: The probability of finding two, three and four jets in the final state as a function of the y_{cut} parameter.

Fig. 3 shows the measured fractions for 2, 3 and 4 jets in the event as a function of the jet resolution parameter, $y_{\rm cut}$ [11], in the region $0.01 < y_{\rm cut} < 0.25$. The rate of dijet reconstruction varies from 70% at $y_{\rm cut} = 0.1$ to 90% at $y_{\rm cut} = 0.2$. The measured jet fractions were compared to jet fractions predicted by SATRAP [14, 15]. SATRAP MC provides a good description of the measurement. Jets were reconstructed with a resolution parameter fixed to $y_{\rm cut} = 0.15$. Events with exactly two reconstructed jets were selected.

3. Results

3.1 Estimate of dijet production with proton dissociation

The contribution of events with a detected dissociated proton system is highly suppressed due to the nominal selection cuts applied to the data, i.e. by requiring exactly two jets, $x_{\mathbb{P}} < 0.01$ and $\eta_{\rm max} < 2$, and has been considered to be negligible. The fraction of events with $\eta_{\rm max} < 2$ associated to the proton-dissociative system, which escaped undetected in the beam hole, was estimated to be $f_{\rm pdiss} = 45\% \pm 4\%({\rm stat.}) \pm 15\%({\rm syst.})$. No evidence was found that $f_{\rm pdiss}$ depends on ϕ or β. Therefore in the following sections a constant amount of proton-dissociative events was subtracted from the selected data sample.

3.2 Unfolding of the hadron-level cross section

An unfolding method was used to obtain hadron-level differential cross sections for production of dijets, reconstructed with jet-resolution parameter $y_{\rm cut} = 0.15$, as a function of β and ϕ in the

following kinematic region: $Q^2 > 25\,\text{GeV}^2$; $90 < W < 250\,\text{GeV}$; $x_{\mathbb{P}} < 0.01$; $M_X > 5\,\text{GeV}$; $N_{\text{jets}} = 2$; $p_{T,\text{jet}} > 2\,\text{GeV}$.

The unfolding was performed by calculating a detector response matrix, which represents a linear transformation of the hadron-level two-dimensional distribution of ϕ–$p_{T,\text{jet}}$ or β–$p_{T,\text{jet}}$ to a detector-level distribution. The unfolding procedure was based on the regularised inversion of the response matrix using Singular Value Decomposition (SVD) as implemented in the TSVDUnfold package [16]. The regularisation parameter was determined according to the procedure suggested by the authors of the unfolding package.

In order to calculate the cross sections for exclusive dijet production, the measured cross sections were scaled by a factor of $(1 - f_{\text{pdiss}}) = 0.55$ according to the estimate of the proton-dissociative background.

3.3 Comparison with model predictions

The differential cross sections were compared to MC predictions for the Resolved-Pomeron model and the Two-Gluon-Exchange model. In the Resolved-Pomeron model [8], the diffractive scattering is factorised into a Pomeron flux from the proton and the hard interaction between the virtual photon and a constituent parton of the Pomeron.

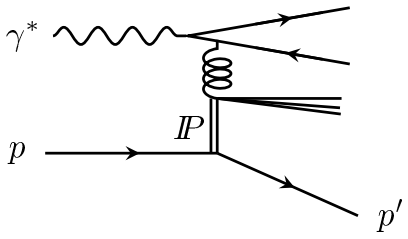

Figure 4: Diagram of diffractive boson–gluon fusion in the Resolved-Pomeron model.

An example of such a process is shown in Fig. 4, where a $q\bar{q}$ pair is produced by a boson–gluon fusion (BGF) process associated with the emission of a Pomeron remnant. This model requires the proton diffractive gluon density as an input for the calculation of the cross section. The predictions considered in this article are based on the parameterisation of the diffractive gluon density obtained from fits (H1 2006 fits A and B) to H1 inclusive diffractive data [17]. The shape of the ϕ distribution is essentially identical in all models based on the BGF process, including both the Resolved-Pomeron and the Soft Colour Interactions (SCI) model [18].

Figure 5: Diagrams of $q\bar{q}$ and $q\bar{q}g$ production in the Two-Gluon-Exchange model.

In the Two-Gluon-Exchange model [6, 4, 7, 5], the diffractive production of a $q\bar{q}$ pair is due to the exchange of a two-gluon colour-singlet state. The process is schematically shown in Fig. 5. The $q\bar{q}$ pair hadronises into a dijet final state. For large diffractive masses, i.e. at low values of β, the cross section for the production of a $q\bar{q}$ pair with an extra gluon is larger than that of the $q\bar{q}$

production. The diagram of this process is also shown in Fig. 5. The $q\bar{q}g$ final state also contributes to the dijet event sample if two of the partons are not resolved by the jet algorithm.

3.4 Differential cross-sections

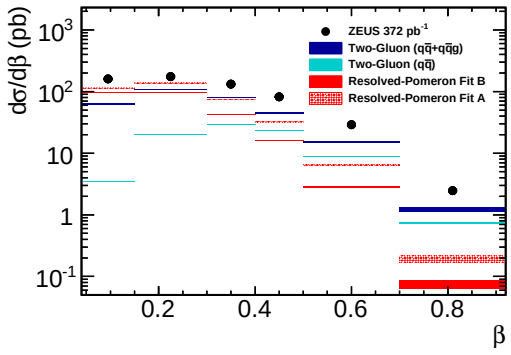

Figure 6: Differential cross sections in comparison to model predictions $\mathrm{d}\sigma/\mathrm{d}\beta$

The cross-section $\mathrm{d}\sigma/\mathrm{d}\beta$ is shown in Fig. 6 together with the predictions from both models. The prediction of the Resolved-Pomeron model decreases with increasing β faster than the measured cross section, for both fit A and fit B. The difference between data and prediction is less pronounced for fit A than for fit B, which is consistent with the observation that the ratio of gluon densities increases with increasing β [17]. Predictions and data differ by a factor of two for small values of β and about ten for large values.

The Two-Gluon-Exchange model prediction, which includes $q\bar{q}$ and $q\bar{q}g$, describes the shape of the measured β distribution reasonably well. The predicted integrated cross section is $\sigma = 38$ pb, while the measured cross section is $\sigma = 72$ pb with a normalisation uncertainty originating from the proton-dissociation background of $u(f_{\mathrm{pdiss}})/(1-f_{\mathrm{pdiss}}) = 27\%$, where $u(f_{\mathrm{pdiss}})$ is the uncertainty in the fraction of events with a dissociated proton. Although the difference between the predicted and measured cross section is not significant, it could indicate that the NLO corrections are large or the cross-section enhancement arising from the evolution of the off-diagonal gluon distribution is significant [19]. The prediction based on $q\bar{q}$ production alone fails to describe the shape of the distribution at low values of β but is almost sufficient to describe it at large β, where the $q\bar{q}g$ component is less important.

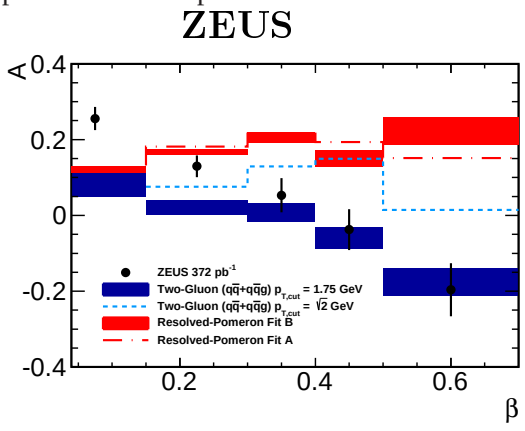

Figure 7: The shape parameter A as a function of β in comparison to the values of A obtained from distributions predicted by the Resolved-Pomeron model and the Two-Gluon-Exchange model

The cross-sections $\mathrm{d}\sigma/\mathrm{d}\phi$ are calculated in five different β ranges. The comparison of the shapes has been quantified by calculating the slope parameter A. The results are shown in Fig. 7. The Resolved-Pomeron model predicts an almost constant, positive value of A in the whole β range. The Two-Gluon-Exchange model ($q\bar{q}+q\bar{q}g$) predicts a value of A which varies from positive to negative. In contrast to the Resolved-Pomeron model, the Two-Gluon-Exchange model agrees quantitatively with the data in the range $0.3 < \beta < 0.7$. The prediction based on $q\bar{q}$ production alone describes the shape of the distributions at large β, where the $q\bar{q}g$ component is less important.

4. Summary

The first measurement of diffractive production of exclusive dijets in deep inelastic scattering, $\gamma^* + p \to \text{jet1} + \text{jet2} + p$, was presented. The differential cross-sections $\mathrm{d}\sigma/\mathrm{d}\beta$ and $\mathrm{d}\sigma/\mathrm{d}\phi$ in bins of β were measured in the kinematic range: $Q^2 > 25\,\mathrm{GeV}^2$, $90 < W < 250\,\mathrm{GeV}$, $M_X > 5\,\mathrm{GeV}$, $x_{\mathbb{P}} < 0.01$ and $p_{T,\mathrm{jet}} > 2\,\mathrm{GeV}$ using an integrated luminosity of 372 pb^{-1}.

The measured absolute cross sections are larger than those predicted by both the Resolved-Pomeron and the Two-Gluon-Exchange models. The difference between the data and the Resolved-Pomeron model at $\beta > 0.4$ is significant. The Two-Gluon-Exchange model predictions agree with the data within the experimental uncertainty and are themselves subject to possible large theoretical uncertainties. The shape of the ϕ distributions was parameterised with the function $1 + A\cos 2\phi$, as motivated by theory. The Two-Gluon-Exchange model predicts reasonably well the measured value of A as a function of β, whereas the Resolved-Pomeron model exhibits a different trend.

References

[1] T. Aaltonen et al., Phys. Rev. **D 77**, 052004 (2008)

[2] A.D. Martin, M.G. Ryskin and V.A Khoze, Phys. Rev. **D 56**, 5867 (1997)

[3] A.S.V. Goloskokov, Phys. Rev. **D 70**, 034011 (2004)

[4] J. Bartels et al., Phys. Lett. **B 386**, 389 (1996)

[5] V.M. Braun and D.Yu. Ivanov, Phys. Rev. **D 72**, 034016 (2005)

[6] J. Bartels, H. Lotter and M. Wüsthoff, Phys. Lett. **B 379**, 239 (1996)

[7] J. Bartels, H. Jung and M. Wüsthoff, Eur. Phys. J. **C 11**, 111 (1999)

[8] G. Ingelman and P.E. Schlein, Phys. Lett. **B 152**, 256 (1985)

[9] G.M. Briskin, Ph.D. Thesis, Tel Aviv University, Report DESY-THESIS 1998-036, 1998

[10] N. Tuning, Ph.D. Thesis, Amsterdam University, 2001

[11] S. Catani et al., Phys. Lett. **B 269**, 432 (1991)

[12] S. Catani et al., Nucl. Phys. **B 406**, 187 (1993)

[13] M. Cacciari, G.P. Salam and G. Soyez, Eur. Phys. J. **C 72**, 1896 (2012)

[14] K. Golec-Biernat and M. Wüsthoff, Phys. Rev. **D 59**, 014017 (1999)

[15] K. Golec-Biernat and M. Wüsthoff, Phys. Rev. **D 60**, 114023 (1999)

[16] A. Hocker and V. Kartvelishvili, Nucl. Instr. and Meth. **A 372**, 469 (1996)

[17] H1 Collab., A. Aktas et al., Eur. Phys. J. **C 48**, 715 (2006)

[18] A. Edin, G. Ingelman and J. Rathsman, Phys. Lett. **B 366**, 371 (1996)

[19] K.J. Golec-Biernat, J. Kwiecinski and A.D. Martin, Phys. Rev. **D 58**, 094001 (1998)